Dean Vortices with Wall Flux in a Curved Channel Membrane System: 2. The Velocity Field

Kun Yong Chung, Mary E. Brewster, and Georges Belfort
Bioseparations Research Center, Howard P. Isermann Dept. of Chemical Engineering,
Rennselaer Polytechnic Institute, Troy, NY 12180

The velocity and pressure fields and the effect of wall flux on these fields in a spiral channel are presented. As fluid flows inward through a spiral channel with constant gap and permeable walls, the streamwise flux decreases while the curvature increases. Thus, by balancing the stabilizing effect of wall suction with the destabilizing effect of increasing curvature, established vortices can be maintained along the spiral channel. This approach is used to prescribe spiral geometries with different wall fluxes. Using a weakly nonlinear stability analysis, the influence of wall flux on the characteristics of Dean vortices is obtained. The critical Dean number is reduced when suction is through the inner wall only, is slightly reduced when suction is equal through both walls, and is increased when suction is through the outer wall only. The magnitude of change is proportional to a ratio of small numbers that measures the importance of the effect of curvature. In membrane filtration applications the wall flux is typically 2 to 5 orders of magnitude less than the streamwise flow. If the radius of curvature of the channel is of the order of 100 times the channel gap, the effect on the critical Dean number is within 2% of the no-wall flux case. If the radius of curvature is sufficiently large, however, it is possible to observe effects on the critical Dean number that approach O(1) in magnitude for certain parameter ranges.

Introduction

In most commercial applications of membrane filtration, the feed solution or suspension is passed tangentially across the membrane surface (often called crossflow) in order to impose sufficient wall shear rate to reentrain retained molecules or particles from the interface back into the bulk solution or suspension. To reduce concentration polarization (buildup of solute at the solution–membrane interface) and fouling, researchers have considered many methods for lowering the concentration gradient between the membrane surface and the bulk fluid and for reentraining solids deposited onto the membrane surface. These include chemical modification of the membrane surface, physical methods such as scouring with sponge balls, and hydrodynamic methods such as the use of eddies during turbulent flow. All these methods, except the modification of membrane surfaces, are based on increasing the mass transfer of suspended and dissolved solids from the membrane solution interface back to the bulk liquid. One of the most successful depolarizing methods has been the use of Taylor vortices established in a rotating annular filter. The main limitations of this type of design are the difficulty in scaling-up membrane area and the high consumption of energy (Belfort, 1988). Consequently, we have presented another method of establishing vortices resulting from the onset of unstable flow in a spiral wound membrane channel (Brewster et al., 1993). Such Dean vortex flow has similar advantages to Taylor vortex flow but is also amenable to scale-up. In addition, it is not expected to consume unreasonable amounts of energy.

The results presented here are part of a larger effort to predict and measure the behavior of Dean vortices in prescribed curved ducts using sophisticated analytical techniques together with magnetic resonance imaging methods. More specifically, we need the velocity and pressure fields (1) to accurately define the spiral geometry that will maintain Dean

Correspondence concerning this article should be addressed to G. Belfort.
Present addresses of: K. Y. Chung, CFC Alternatives Technology Center, KIST, P.O. Box 131, Cheongryang, Seoul 130-650, Korea; M. E. Brewster, Battelle Pacific Northwest Labs., P. O. Box 999, Richland, WA 99352.

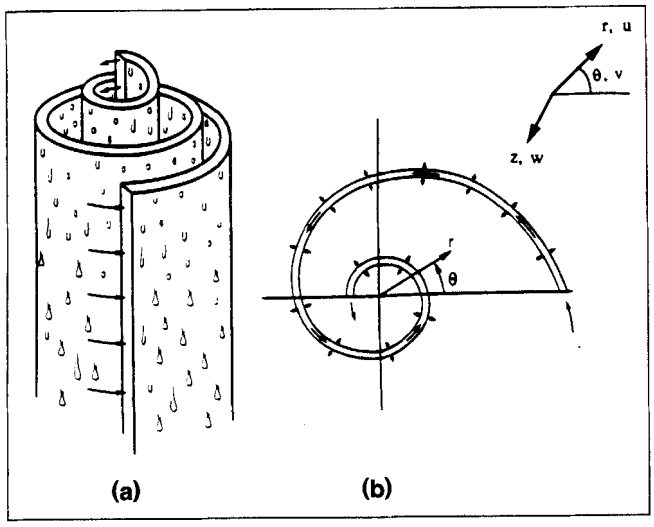

Figure 1. (a) Flow through a spiral porous channel; (b) cross section of spiral channel and definition of coordinates.

vortices throughout the streamwise path, and (2) to solve the convective-diffusion equation to obtain the solute concentration profiles within the duct (Chung et al., 1994). Our eventual purpose is to use this know-how for developing a new membrane module (Figure 1) in which Dean vortex flow will depolarize the buildup of dissolved and suspended solutes at the membrane–solution interface (Belfort et al., 1993). Modules with variable gap width have recently been designed that have surface-area packing density equivalent to commercial modules such as axial-flow spiral wound modules (Brewster et al., 1994).

Membrane filtration aside, the spiral channel is also of interest as a fundamental problem in fluid mechanics. A centrifugal instability created by a negative radial pressure gradient is perturbed by radial flow due to wall suction. In this study, the velocity field and the effect of wall flux on these fields in a spiral channel are presented.

At sufficiently small Reynolds numbers, the velocity in curved channel flow is purely streamwise. Its profile is similar to the parabolic profile of plane channel flow, but the location of maximum velocity is shifted toward the outer wall. At higher Reynolds numbers, centrifugal instabilities cause a secondary flow containing streamwise-oriented Dean vortices (Dean, 1928). Dean vortices occur in regularly spaced counterrotating pairs. However, a transition to unsteady secondary flow has been observed for Dean numbers slightly above De_c; in particular, this transition was observed at $1.2De_c$ for $\eta = 0.975$ (Finlay et al., 1988). The Dean number is defined as $De = Re\sqrt{2d/r_i}$, where the Reynolds number, $Re = dV/\nu$, and the radius ratio, $\eta = r_i/r_o$. For $De > De_c$, Dean vortices are also unstable to merging and splitting (Guo and Finlay, 1991). As fluid flows through a spiral channel with permeable walls, the streamwise flux decreases, thereby stabilizing curved channel Poiseuille flow (hereafter referred as CCPF). If the channel spirals inward, the curvature increases. This destabilizes CCPF. Thus, by balancing the stabilizing effect of wall suction with the destabilizing effect of increasing curvature, established vortices can be maintained along the flow path (Figure 1).

In the following section, we present the mathematical approach including the assumptions on which the model is based, nondimensionalized expressions for the continuity and momentum equations with the narrow-gap approximation, and the associated boundary conditions. A weakly nonlinear analysis for solving this problem is described in the next section. The results in the nonporous case are then compared with a wide-gap solution and a fully nonlinear solution to determine the preciseness of the approach. Finally, the main conclusions are summarized.

Mathematical Approach

The Navier–Stokes equations with appropriate boundary conditions are solved for viscous fluid flow in a spiral channel with porous walls. To simplify and to make the problem more tractable, the following assumptions are made:

- The fluid is incompressible and Newtonian under isothermal conditions.
- Fully developed steady flow enters a channel with infinite length and breadth, that is, entrance, exit, and end effects are neglected.
- No-slip conditions exist at the wall. This is realistic for flow in membrane modules in common use (Belfort and Nagata, 1985).
- The gravitational force is negligible.
- The wall flux is constant and small compared to the streamwise flux. Only the first-order wall-flux effect is considered. This assumption is reasonable for commercial pressure-driven membrane processes, where cross-flow is usually far larger than permeation flow (by factor of 10^2 to 10^5).
- The flow is "slowly varying" in the streamwise direction. Thus we scale the polar angle θ to obtain $\varphi = \gamma_I \theta$, where γ_I is a small parameter (Table 1). Further, the shape of the constant gap spiral channel is defined by

$$r_c = r_{cI} K(\varphi)$$

so that locally the channel acts as an uniformly curved channel. The velocity components v, w are taken to be parallel to the channel walls while u is taken to be perpendicular. Because the channel is almost uniformly curved, these velocity components are equivalent to the components in cylindrical coordinates in the first approximation. Thus we suppose that the velocity field satisfies the Navier–Stokes equations in cylindrical coordinates.

The dimensional continuity and Navier–Stokes equations in cylindrical coordinates are summarized as follows:

Continuity Equation:

$$\frac{1}{r}\frac{\partial(ru)}{\partial r} + \frac{1}{r}\frac{\partial v}{\partial \theta} + \frac{\partial w}{\partial z} = 0. \tag{1}$$

Equations of Motion:

Table 1. Dimensionless Parameters and Variables*

$\chi = \dfrac{r - r_c}{d}$	$\zeta = \dfrac{z}{d}$	$\tau = \dfrac{t}{d^2/\nu}$	$\epsilon = \dfrac{u_w}{V_I}$
$\gamma_I = \dfrac{\epsilon}{\delta_I^2}$		$\varphi = \gamma_I \theta$	$\Psi = \dfrac{1}{1+2\varphi}$
$\eta = \dfrac{r_i}{r_o}$	$\delta^2 = 1 - \eta$	$r = r_c + O(\delta_I^2)$	
$d/r_c = \dfrac{1-\eta}{1+\eta} \doteq \dfrac{\delta^2}{2}$	$K = \dfrac{r_c}{r_{cI}} \doteq \dfrac{\delta_I^2}{\delta^2}$	$Re(\theta) = \dfrac{V(\theta)d}{\nu}$	$De(\theta) = 2Re(\theta)\delta(\theta)$
$\tilde{v} = \dfrac{v}{V_I}$	$\tilde{v} = \mathrm{B}(\varphi)\bar{v}(\zeta)$	$V(\theta) = \dfrac{1}{2d}\int_{r_i}^{r_o} v(r)\,dr$	
$\tilde{u} = (De_I\delta_I)^{-1}\dfrac{u}{V_I}$	$\tilde{w} = (De_I\delta_I)^{-1}\dfrac{w}{V_I}$	$\tilde{p} = \dfrac{p}{\rho V_I^2}$	

*Where subscript I refers to the inlet.

$$\frac{\partial u}{\partial t} + u\frac{\partial u}{\partial r} + \frac{v}{r}\frac{\partial u}{\partial \theta} - \frac{v^2}{r} + w\frac{\partial u}{\partial z} = -\frac{1}{\rho}\frac{\partial p}{\partial r} + \nu\left[\frac{\partial}{\partial r}\left(\frac{1}{r}\frac{\partial}{\partial r}(ru)\right) + \frac{1}{r^2}\frac{\partial^2 u}{\partial \theta^2} - \frac{2}{r^2}\frac{\partial v}{\partial \theta} + \frac{\partial^2 u}{\partial z^2}\right], \quad (2)$$

$$\frac{\partial v}{\partial t} + u\frac{\partial v}{\partial r} + \frac{v}{r}\frac{\partial v}{\partial \theta} - \frac{uv}{r} + w\frac{\partial v}{\partial z} = -\frac{1}{\rho r}\frac{\partial p}{\partial \theta} + \nu\left[\frac{\partial}{\partial r}\left(\frac{1}{r}\frac{\partial}{\partial r}(rv)\right) + \frac{1}{r^2}\frac{\partial^2 v}{\partial \theta^2} + \frac{2}{r^2}\frac{\partial u}{\partial \theta} + \frac{\partial^2 v}{\partial z^2}\right], \quad (3)$$

$$\frac{\partial w}{\partial t} + u\frac{\partial w}{\partial r} + \frac{v}{r}\frac{\partial w}{\partial \theta} + w\frac{\partial w}{\partial z} = -\frac{1}{\rho}\frac{\partial p}{\partial z} + \nu\left[\frac{1}{r}\frac{\partial}{\partial r}\left(r\frac{\partial w}{\partial r}\right) + \frac{1}{r^2}\frac{\partial^2 w}{\partial \theta^2} + \frac{\partial^2 w}{\partial z^2}\right]. \quad (4)$$

The continuity and Navier–Stokes equations are nondimensionalized using the definitions in Table 1. The approach is similar to that followed by Chandrasekhar (1961) and Drazin and Reid (1981) except that wall flux is introduced into the problem for the first time. There are two-dimensionless parameters that affect the approximations we now make to the governing equations (Eqs. 1–4). The first,

$$\delta = [1-\eta]^{0.5} = \left(\frac{2d}{r_0}\right)^{0.5},$$

is a geometric parameter relating the radius of curvature of the spiral to its gap height. This parameter is assumed small ($\delta \ll 1$); that is, we assume the gap is small compared to the radius of curvature of the spiral. This is called the "narrow-gap approximation." The second,

$$\gamma = \frac{\epsilon}{\delta_I^2} = \frac{1}{\delta_I^2}\frac{u_w}{V_I},$$

is roughly the ratio of the flux from suction through the walls in one turn of the spiral to the streamwise flux in the spiral (in the θ direction) divided by the geometric parameter. For the general analysis of the interaction of wall suction with centrifugal instabilities, this parameter is not assumed small. However, we do assume

$$\gamma\delta_I \ll 1$$

and

$$\delta_I \ll \gamma.$$

In the perturbation expansion of the governing equations based on $\delta_I \ll 1$ and $\gamma\delta_I \ll 1$, we retain terms of $O(\gamma\delta_I)$, neglecting terms of smaller order including $O(\delta_I^2)$ and $O(\gamma^2\delta_I^2)$. We note that for any more accurate treatment of this problem the Navier–Stokes equations must be expressed in terms of curvilinear coordinates fitted to the spiral geometry. For example, the transverse velocity u is only approximately radial, although at our level of approximation, it is considered to be the radial velocity.

Assuming that the width of the gap between the membranes is much smaller than the radii of curvature of the two walls or that the ratio r_i/r_o is close to 1, terms in the full equations containing δ_I^2 can be neglected. With this narrow-gap approximation, a revised set of momentum and continuity equations are obtained. These, together with their boundary conditions, are described below.

Continuity Equation:

$$\frac{\partial \tilde{u}}{\partial \chi} + \frac{1}{2De}\gamma_I\delta_I K^{-1}\frac{\partial \tilde{v}}{\partial \varphi} + \frac{\partial \tilde{w}}{\partial \zeta} = 0 + O(\delta_I^2). \quad (5)$$

Equations of Motion:

$$\frac{\partial \tilde{u}}{\partial \tau} + \frac{1}{2}De^2\tilde{u}\frac{\partial \tilde{u}}{\partial \chi} + \frac{1}{4}De\gamma_I\delta_I K^{-1}\tilde{v}\frac{\partial \tilde{u}}{\partial \varphi} + \frac{1}{2}De^2\tilde{w}\frac{\partial \tilde{u}}{\partial \zeta} - \frac{1}{4}K^{-1}\tilde{v}^2 = -\frac{1}{2\delta_I^2}\frac{\partial \tilde{p}}{\partial \chi} + \frac{\partial^2 \tilde{u}}{\partial \zeta^2} + \frac{\partial^2 \tilde{u}}{\partial \chi^2} + O(\delta_I^2), \quad (6)$$

$$\frac{\partial \tilde{v}}{\partial \tau}+\frac{1}{2}De^2\tilde{u}\frac{\partial \tilde{v}}{\partial \chi}+\frac{1}{4}De\gamma_I\delta_I K^{-1}\tilde{v}\frac{\partial \tilde{v}}{\partial \varphi}+\frac{1}{2}De^2\tilde{w}\frac{\partial \tilde{v}}{\partial \zeta}$$

$$=-\frac{1}{4}De\gamma_I\delta_I K^{-1}\frac{\partial \tilde{p}}{\partial \varphi}+\frac{\partial^2 \tilde{v}}{\partial \zeta^2}+\frac{\partial^2 \tilde{v}}{\partial \chi^2}+O(\delta_I^2), \quad (7)$$

$$\frac{\partial \tilde{w}}{\partial \tau}+\frac{1}{2}De^2\tilde{u}\frac{\partial \tilde{w}}{\partial \chi}+\frac{1}{4}De\gamma_I\delta_I K^{-1}\tilde{v}\frac{\partial \tilde{w}}{\partial \varphi}+\frac{1}{2}De^2\tilde{w}\frac{\partial \tilde{w}}{\partial \zeta}$$

$$=-\frac{1}{2\delta_I^2}\frac{\partial \tilde{p}}{\partial \zeta}+\frac{\partial^2 \tilde{w}}{\partial \zeta^2}+\frac{\partial^2 \tilde{w}}{\partial \chi^2}+O(\delta_I^2). \quad (8)$$

Boundary Conditions:

$$\chi=+1 \text{ (outer wall)} \quad \tilde{u}=\frac{1}{De}(+1-\beta), \quad \tilde{v}=\tilde{w}=0, \quad (9)$$

$$\chi=-1 \text{ (inner wall)} \quad \tilde{u}=\frac{1}{De}(-1-\beta), \quad \tilde{v}=\tilde{w}=0, \quad (10)$$

where β is the wall flux partition factor ($-1\le\beta\le+1$). Note that for $\beta=1$ the inner wall is permeable only, for $\beta=-1$ the outer wall is permeable only, and for $\beta=0$ both walls are permeable with equal flux.

Solution Method

Finlay et al. (1988) solved the weakly nonlinear problem for flow in a nonporous curved channel that followed the procedure given by DiPrima (1967) for the Taylor vortex problem. Fourier series expressions for the velocities (u, v, and w) and pressure were used. These equations were substituted into the Navier–Stokes equations with the required initial and boundary conditions.

A similar approach to Finlay et al. (1988) is followed here except for two differences. The first difference is that here constant wall suction rate at the curved walls is applied while Finlay et al. (1988) used solid walls. This means that unlike the uniform channel with nonporous walls, the solution of our problem is in fact not constant in the streamwise direction. The second difference is that here the nondimensional equations are truncated using the narrow-gap approximations, whereas Finlay et al. (1988) treats the wide-gap case. Consequently, the continuity and Navier–Stokes equations are nondimensionalized with parameters that are different from those used by Finlay et al. (1988) and are similar to those used by Dean (1928), these being most appropriate for the narrow-gap case.

We now consider secondary motion that arises as we increase the Dean number. The linear stability analysis of the uniformly curved channel with nonporous walls was first carried out by Dean (1928), who observed an instability to axisymmetric perturbations periodic in z. This instability has been shown theoretically to be the primary instability provided that radius ratio $\eta\le 1-2.179\times10^{-5}$ (Gibson and Cook, 1974). Experimental evidence supports these results (Brewster et al., 1959). Thus we consider only perturbations to the velocities that are axisymmetric and periodic in ζ with a specified wavenumber a. We will show that it is possible to make this assumption provided the Dean number is constant along the channel.

The dimensionless velocities $\tilde{u}$, $\tilde{v}$, $\tilde{w}$ and the dimensionless pressure $\tilde{p}$ are expanded in a regular perturbation as follows

$$\tilde{u}(\tau,\zeta,\varphi,\chi)=\tilde{u}^0+\gamma_I\delta_I\tilde{u}^1+\cdots,$$

$$\tilde{v}(\tau,\zeta,\varphi,\chi)=\tilde{v}^0+\gamma_I\delta_I\tilde{v}^1+\cdots,$$

$$\tilde{w}(\tau,\zeta,\varphi,\chi)=\tilde{w}^0+\gamma_I\delta_I\tilde{w}^1+\cdots,$$

$$\tilde{p}(\tau,\zeta,\varphi,\chi)=\frac{1}{\gamma_I\delta_I}\tilde{p}^{00}(\tau,\varphi)+\tilde{p}^{01}(\tau,\varphi)$$

$$+\delta_I^2\tilde{p}^1(\tau,\zeta,\varphi,\chi)+\gamma_I\delta_I^3\tilde{p}^2(\tau,\zeta,\varphi,\chi)+\cdots. \quad (11)$$

The form of the pressure expansion is brought about because the primary pressure gradient in the φ direction is much larger than the secondary pressure gradients in the χ and ζ directions. The terms of order higher than $(\gamma_I\delta_I)$ in Eqs. 11 are neglected because the wall flux is very small compared to the streamwise velocity (two to five orders of magnitude smaller).

We now use the assumption of periodicity in ζ to expand the velocity components into Fourier series. Because of the symmetry of the problem in the z direction, it is sufficient to let velocity components $\tilde{u}$, $\tilde{v}$ and pressure $\tilde{p}$ be even functions of ζ, and let $\tilde{w}$ (according to the continuity equation) be an odd function of ζ (Finlay et al., 1988; DiPrima, 1967):

$$\tilde{u}^0=\sum_{n=1}^{\infty}\tilde{u}_n^0\cos(na\zeta), \quad \tilde{u}^1=\sum_{n=0}^{\infty}\tilde{u}_n^1\cos(na\zeta),$$

$$\tilde{v}^0=\sum_{n=0}^{\infty}\tilde{v}_n^0\cos(na\zeta), \quad \tilde{v}^1=\sum_{n=1}^{\infty}\tilde{v}_n^1\cos(na\zeta),$$

$$\tilde{w}^0=\sum_{n=0}^{\infty}\tilde{w}_n^0\sin(na\zeta), \quad \tilde{w}^1=\sum_{n=1}^{\infty}\tilde{w}_n^1\sin(na\zeta),$$

$$\tilde{p}^1=\sum_{n=0}^{\infty}\tilde{p}_n^1\cos(na\zeta), \quad \tilde{p}^2=\sum_{n=1}^{\infty}\tilde{p}_n^2\cos(na\zeta). \quad (12)$$

We begin by finding the terms in Eq. 12 that are independent of ζ. We assume these are also independent of time. Further, the primary streamwise velocity $\tilde{v}_0^0$ is assumed to retain the same profile, but the absolute value decreases due to the mass balance and is separable into velocity scaling factor and velocity profile function, $\tilde{B}(\varphi)$ and $\bar{v}$, respectively

$$\tilde{v}_0^0(\chi,\varphi)=\tilde{B}(\varphi)\bar{v}_0^0(\chi). \quad (13)$$

The justification for these assumptions is that it is possible to obtain a solution of this form and this solution corresponds to the unperturbed steady state. $\tilde{B}(\varphi)$ is obtained from integration of the continuity equation. At $O(\gamma_I\delta_I)$ and index in Fourier expansion, $n=0$, the continuity equation becomes

$$\frac{\partial \tilde{u}_0^1}{\partial \chi}+\frac{K^{-1}}{2De}\frac{\partial \tilde{v}_0^0}{\partial \varphi}=0. \quad (14)$$

By integrating the leading order term of Eq. 13 from $\zeta=-1$ to $\zeta=1$, we obtain

$$\tilde{B}(\varphi)=\frac{1}{2}\int_{-1}^{1}\tilde{v}_0^0\,d\chi. \tag{15}$$

Then

$$\frac{1}{2}\int_{1}^{-1}\frac{\partial\tilde{u}_0^1}{\partial\chi}d\chi+\frac{K^{-1}}{2De}\tilde{B}'(\varphi)=0. \tag{16}$$

The first term in Eq. 16 is integrated with boundary conditions (Eqs. 9 and 10):

$$\frac{1}{2}\int_{-1}^{1}\frac{\partial\tilde{u}_0^1}{\partial\chi}d\chi=De^{-1}. \tag{17}$$

Substituting Eq. 17 into Eq. 16, we obtain

$$\tilde{B}'(\varphi)=-2K. \tag{18}$$

In addition, the leading order term for centrifugal acceleration $\tilde{v}^2K^{-1}$ in Eq. 6 is assumed to be independent of φ to maintain the same Dean vortex strength through the curved channel. Thus $\tilde{B}^2K^{-1}=$ constant, but $\tilde{B}(0)=1$ and $K(0)=1$. Finally,

$$\tilde{B}^2K^{-1}=1 \quad \text{or} \quad \tilde{B}^2=K. \tag{19}$$

By solving Eqs. 18 and 19 simultaneously, $\tilde{B}(\varphi)$ and $K(\varphi)$ are obtained:

$$\tilde{B}(\varphi)=\frac{1}{1+2\varphi}, \tag{20}$$

$$K(\varphi)=\frac{r_c(\varphi)}{r_{cI}}=\frac{1}{(1+2\varphi)^2}, \tag{21}$$

where $K(\varphi)$ is the ratio of centered radius at a certain φ to that at the inlet. Thus a mathematical expression for a spiral configuration is obtained. Different spiral shapes are shown in Figure 2a and b when the ratio of the permeation to the mean streamwise velocity at the inlet, ϵ, are 10^{-4} and 5×10^{-5}, respectively.

The streamwise velocity $\tilde{v}_0^0$ and pressure drop $(\partial\tilde{p}_0^{00}/\partial\varphi)$ for CCPF (i.e., no wall flux, so that $\tilde{B}(\varphi)=1$) are obtained with no-slip boundary conditions and Eq. 15 as follows,

$$\tilde{v}_0^0=\frac{3}{2}(1-\chi^2), \tag{22}$$

$$\frac{\partial\tilde{p}_0^{00}}{\partial\varphi}=-\frac{12\tilde{B}K}{De}. \tag{23}$$

The continuity equation (Eq. 5) at $O(\gamma_I\delta_I)$ becomes

$$\frac{\partial\tilde{u}_0^1}{\partial\chi}-\frac{\tilde{v}_0^0}{De}=0. \tag{24}$$

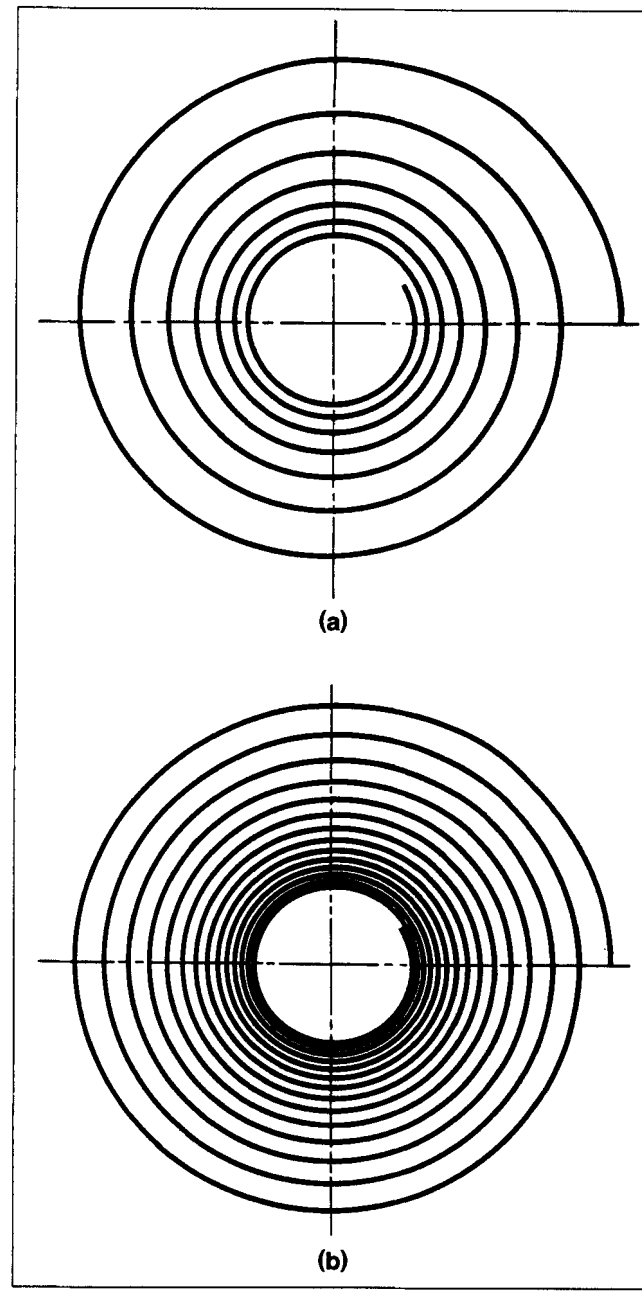

Figure 2. Spiral configurations based on $K=1/(1+2\varphi)^2$ for (a) $\epsilon=10^{-4}$ and (b) $\epsilon=5\times10^{-5}$.

The radius ratio η varies from 0.990 to 0.965.

Substituting Eq. 22 into Eq. 24 and integrating with the boundary conditions (Eqs. 9 and 10) gives

$$\tilde{u}_0^1=\frac{1}{De}\left(\frac{3}{2}\chi-\frac{1}{2}\chi^3-\beta\right). \tag{25}$$

$\tilde{v}_0^1$ and pressure drop $(\partial\tilde{p}_0^{01}/\partial\varphi)$ are obtained from φ-momentum Eq. 7 at $O(\gamma_I\delta_I)$:

$$D^2\tilde{v}_0^{-1}=\frac{1}{2}De^2\tilde{u}_0^1D\tilde{v}_0^0-\frac{1}{2}De(\tilde{v}_0^0)^2+\frac{De}{4\tilde{B}K}\frac{\partial\tilde{p}_0^{01}}{\partial\varphi} \tag{26}$$

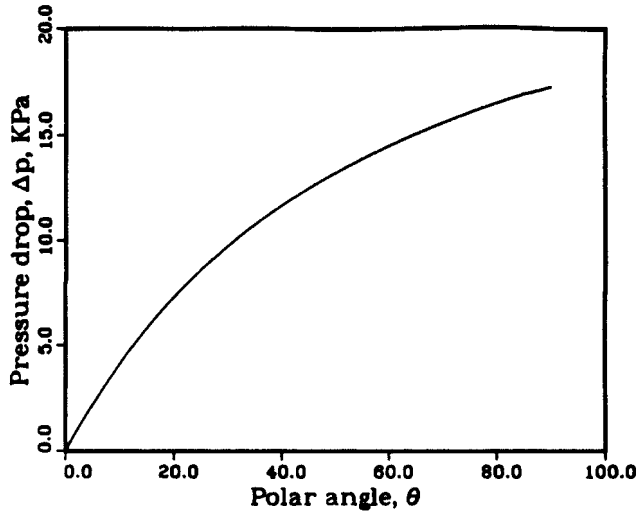

Figure 3. Dimensional pressure drop Δp along a spiral porous channel for $De = 1.1De_c$, $\epsilon = 5\times10^{-5}$, $r_{cl} = 10$ cm, $d_l = 0.05$ cm, and $\eta_l = 0.99$.

and the condition $\int_{-1}^{1}\bar{v}_0^1\,d\chi = 0$, which corresponds to the assumption of zero net flow through the (r, z) plane. Thus,

$$\bar{v}_0^1 = De\left(-\frac{1}{80}\chi^6 + \frac{9}{560}\chi^2 - \frac{1}{280}\right) + \frac{De\beta}{4}(\chi^3 - \chi) \quad (27)$$

and

$$\frac{\partial\tilde{p}_0^{01}}{\partial\varphi} = \frac{162\tilde{B}K}{35}. \quad (28)$$

Finally, the pressure drop can be obtained from Eqs. 11, 23, and 28 as

$$\Delta\tilde{p} = \frac{1}{\gamma_l\delta_l}\Delta\tilde{p}_0^{00} + \Delta\tilde{p}_0^{01} = (K-1)\left(\frac{3}{\gamma_l\delta_l De} - \frac{81}{70}\right). \quad (29)$$

As an illustration of a pressure-drop calculation in a typical spiral membrane filtration application, let $De = 40$, $\epsilon = 5\times10^{-5}$, $r_{cl} = 10$ cm, $d_l = 0.05$ cm, and $\eta_l = 0.99$, $(3/\gamma_l\delta_l De) - (81/70)$ gives 149.2, and as the dimensionless $\Delta\tilde{p}$ converts into dimensional Δp, it gives

$$\Delta p = 23.9(K-1). \quad (30)$$

The dimensional pressure drop Δp *(KPa)* is shown in Figure 3. This pressure drop does include the effect of wall flux but does not include the effect of Dean vortices.

Now we determine the secondary flow as it is described by the first nonconstant terms in the Fourier series of Eq. 12. Following DiPrima (1967), the unknown variables are expanded in a power series in an as yet unknown vortex amplitude A:

$$Q_n^k(\chi,\tau) = A^k(\tau)\left[Q_{n0}^k(\chi) + \sum_{m=1}^{\infty} A^{2m}(\tau)Q_{nm}^k(\chi)\right], \quad (31)$$

where $Q_{nm}^k = (\tilde{u}_{nm}^k, \bar{v}_{nm}^k)$. The corresponding terms of $\tilde{w}$ and $\tilde{p}$ are obtained from the continuity equation (Eq. 5) and ζ-momentum (Eq. 8) equations, respectively. In order to obtain the vortex amplitude (A), the following series expansion is obtained:

$$dA/d\tau = (\sigma^0 + \gamma_l\delta_l\sigma^1 + \cdots)A + (a_1 + \cdots)A^3 + O(A^5). \quad (32)$$

where we assume $A^2 = O(\sigma_0) = O(\gamma_l\delta_l)$ and we keep terms to $O(A^3)$.

After substituting from Eqs. 11, 12, 31 and 32, the boundary value problem expressed by Eqs. 5–8 can be decomposed into several subproblems summarized in the Appendix. The equation at $O[A^3(\gamma_l\delta_l)^0]$ is discussed by Finlay et al. (1988) for the wide gap case. The value of the Landau coefficient a_1 for the narrow-gap case can be obtained from the wide-gap case in the limit as the radius ratio η tends to 1.

The vortex amplitude (A) includes the wall flux effect, and the first order in $\gamma_l\delta_l$ is enough for an estimate of A because of the small wall flux ratio. At steady state

$$A = \sqrt{\frac{\sigma^0 + \gamma_l\delta_l\sigma^1}{-a_1}}. \quad (33)$$

The revised critical Dean number $\widetilde{De}_c$ occurs when $A = 0$. From Eq. 33, $A = 0$ when $\sigma^0 = -\gamma_l\delta_l\sigma^1$. Since σ^0 is proportional to $\widetilde{De}_c - De_c$ for small σ^0, then we find

$$\widetilde{De}_c - De_c = O(\gamma_l\delta_l) = O\left(\frac{\epsilon}{\delta_l}\right). \quad (34)$$

In particular,

$$\widetilde{De}_c - De_c = -k\gamma_l\delta_l\sigma^1 = -k\sigma^1\frac{\epsilon}{\delta_l}, \quad (35)$$

where

$$k^{-1} = \frac{\partial\sigma^0}{\partial De}(De_c).$$

The first-order growth rate (σ^0) is obtained from the linear stability analysis (Eqs. A5 and A6 in the Appendix). The coefficient k is obtained by numerical differentiation using two evaluations of σ^0 near the critical Dean number. We find $k \sim 8.3$. The perturbation to the first-order growth rate (σ^1), which reflects the wall-flux effect, is obtained from Eqs. A7 and A8 in the Appendix using a solvability criterion (Edelen and Kydoniefs, 1975) as described below. The results are linearly dependent on the wall-flux ratio β. We find $\sigma^1 \sim 30(1 + 2\beta)$. Thus the relative change in the critical Dean number is

$$\frac{\tilde{De}_c - De_c}{De_c} = -6.9(1+2\beta)\frac{\epsilon}{\delta_l}. \quad (36)$$

Solvability Criterion. Homogeneous parts in $O(A^1\gamma_I^1\delta_I^1)$ (Eqs. A7 and A8) are the same as $O(A^1\gamma_I^0\delta_I^0)$. The double precision IMSL subroutine DIVPAG and DZREAL are used to obtain the homogeneous solution as described in detail by Chung (1992). In order to obtain the particular solutions of $O(A^1\gamma_I^1\delta_I^1)$ Eqs. A7 and A8 are divided into two parts as follows:

$$(D^2-a^2-\sigma^0)\bar{v}_{11p}^I-\frac{1}{2}De^2\tilde{u}_{11p}^I D\bar{v}_0^0=\bar{v}_1^0, \tag{37}$$

$$(D^2-a^2-\sigma^0)(D^2-a^2)\tilde{u}_{11p}^I-\frac{1}{2}a^2\bar{v}_0^0\bar{v}_{11p}^I=(D^2-a^2)\tilde{u}_1^0 \tag{38}$$

and

$$(D^2-a^2-\sigma^0)\bar{v}_{11p}^{II}-\frac{1}{2}De^2\tilde{u}_{11p}^{II}D\bar{v}_0^0=\frac{1}{2}De^2\left(\tilde{u}_1^0D\bar{v}_0^1+\tilde{u}_0^1D\bar{v}_1^0\right)-De\bar{v}_0^0\bar{v}_1^0, \tag{39}$$

$$(D^2-a^2-\sigma^0)(D^2-a^2)\tilde{u}_{11p}^{II}-\frac{1}{2}a^2\bar{v}_0^0\bar{v}_{11p}^{II}=\frac{1}{2}a^2\bar{v}_1^0\bar{v}_0^1-\frac{1}{2}a^2De^2\left(\tilde{u}_1^0D\tilde{u}_0^1+\tilde{u}_0^1D\tilde{u}_1^0\right)-\frac{\sigma^0}{De}D\bar{v}_1^0+\frac{De^2}{2}\left(D\tilde{u}_0^1D^2\tilde{u}_1^0+\tilde{u}_0^1D^3\tilde{u}_1^0\right)+\frac{1}{De}(D^3-a^2D)\bar{v}_1^0. \tag{40}$$

Then

$$\tilde{u}_p=\sigma^1\tilde{u}_p^I+\tilde{u}_p^{II} \quad \text{and} \quad \tilde{v}_p=\sigma^1\tilde{v}_p^I+\tilde{v}_p^{II},$$

where subscript p represents the particular solutions.

The particular solution and the three initial value solutions are found using a fourth-order Runge–Kutta method with a Richardson extrapolation. The boundary conditions for the particular solutions are defined as follows:

$$\begin{pmatrix} \tilde{u}_1^0(r_i)=0 \\ D\tilde{u}_1^0(r_i)=0 \\ D^2\tilde{u}_1^0(r_i)=C_1 \\ D^3\tilde{u}_1^0(r_i)=C_2 \\ \bar{v}_1^0(r_i)=0 \\ D\bar{v}_1^0(r_i)=C_3 \end{pmatrix}, \tag{41}$$

and

$$(I)=\begin{pmatrix} \tilde{u}_{11p}^I(r_i)=0 \\ D\tilde{u}_{11p}^I(r_i)=0 \\ D^2\tilde{u}_{11p}^I(r_i)=0 \\ D^3\tilde{u}_{11p}^I(r_i)=0 \\ \bar{v}_{11p}^I(r_i)=0 \\ D\bar{v}_{11p}^I(r_i)=0 \end{pmatrix} \quad \text{or} \quad (II)\begin{pmatrix} \tilde{u}_{11p}^{II}(r_i)=0 \\ D\tilde{u}_{11p}^{II}(r_i)=0 \\ D^2\tilde{u}_{11p}^{II}(r_i)=0 \\ D^3\tilde{u}_{11p}^{II}(r_i)=0 \\ \bar{v}_{11p}^{II}(r_i)=0 \\ D\bar{v}_{11p}^{II}(r_i)=0 \end{pmatrix}, \tag{42}$$

and

$$\tilde{u}_1^1(r_o)=D\tilde{u}_1^1(r_o)=\bar{v}_1^1(r_o)=0. \tag{43}$$

At r_o the linear combination must satisfy the set of linear equations $\boldsymbol{Ac'+d=0}$ where:

$$\boldsymbol{A}\equiv\begin{pmatrix} u^I(r_o) & u^{II}(r_o) & u^{III}(r_o) \\ Du^I(r_o) & Du^{II}(r_o) & Du^{III}(r_o) \\ v^I(r_o) & v^{II}(r_o) & v^{III}(r_o) \end{pmatrix},$$

$$\boldsymbol{c'}=\begin{pmatrix} c_1' \\ c_2' \\ c_3' \end{pmatrix} \quad \text{and} \quad \boldsymbol{d}=\begin{pmatrix} \tilde{u}_p(r_o) \\ D\tilde{u}_p(r_o) \\ \tilde{v}_p(r_o) \end{pmatrix}. \tag{44}$$

Because $\boldsymbol{A}$ is singular, there exists a nontrivial vector $\boldsymbol{e}$ such that

$$(e_1 \quad e_2 \quad e_3)(\boldsymbol{A})=0. \tag{45}$$

Multiplying equation $\boldsymbol{Ac'+d=0}$ by $\boldsymbol{e}$, we obtain

$$\boldsymbol{eAc'}+\boldsymbol{e}\begin{pmatrix} \tilde{u}_p(r_o) \\ D\tilde{u}_p(r_o) \\ \tilde{v}_p(r_o) \end{pmatrix}=\boldsymbol{0}. \tag{46}$$

Substituting Eq. 45 into Eq. 46 yields

$$(e_1 \quad e_2 \quad e_3)\begin{pmatrix} \tilde{u}_p(r_o) \\ D\tilde{u}_p(r_o) \\ \tilde{v}_p(r_o) \end{pmatrix}=0. \tag{47}$$

This is a necessary condition for the solvability of Eqs. A7 and A8. Therefore,

$$\sigma^1=-\frac{e_1\tilde{u}_{11p}^{II}(r_o)+e_2D\tilde{u}_{11p}^{II}(r_o)+e_3\tilde{v}_{11p}^{II}(r_o)}{e_1\tilde{u}_{11p}^{I}(r_o)+e_2D\tilde{u}_{11p}^{I}(r_o)+e_3\tilde{v}_{11p}^{I}(r_o)}. \tag{48}$$

Also notice that the dependence of σ^1 on the wall-flux partition factor β enters via a linear dependence on $\tilde{u}_0^1$, which in turn depends linearly on β. Thus perturbation to the linear growth rate σ^1 depends linearly on the wall-flux partition factor β.

We now consider the effect of wall suction on the critical wavenumber. In a nonporous channel, the linear growth rate σ is a function of Dean number, De, and wavenumber a. The critical Dean number, $De_c(a)$ is the value of the Dean number that gives a zero value of σ for a specified wavenumber. That is

$$\sigma[De_c(a),a]=0. \tag{49}$$

The critical wavenumber, a_c, is characterized as that value of a that gives a minimum of the critical Dean number, $De_c(a)$. That is,

$$\frac{dDe_c}{da}(a_c) = 0. \tag{50}$$

Differentiation of Eq. 49 by a gives

$$\frac{\partial \sigma}{\partial De}\frac{dDe_c}{da} + \frac{\partial \sigma}{\partial a} = 0. \tag{51}$$

At the critical wave number, a_c, we thus have

$$\frac{\partial \sigma}{\partial a}[De_c(a_c), a_c] = 0. \tag{52}$$

When we introduce wall suction, according to the parameter ϵ, the linear growth rate is affected and, hence, the critical Dean number and the critical wavenumber will change slightly. Let the revised critical Dean number be $\tilde{De}(a, \epsilon)$. Then

$$\sigma[\tilde{De}(a, \epsilon), a, \epsilon] = 0. \tag{53}$$

Further, let the revised critical wavenumber $\tilde{a}(\epsilon)$ be such that

$$\left[\frac{\partial \tilde{De}}{\partial a}\right]_{\epsilon}[\tilde{a}(\epsilon), \epsilon] = 0. \tag{54}$$

Then differentiating Eq. 53 with respect to a (ϵ fixed) gives

$$\frac{\partial \sigma}{\partial De}\frac{\partial \tilde{De}}{\partial a} + \frac{\partial \sigma}{\partial a} = 0. \tag{55}$$

Evaluating Eq. 55 at $a = \tilde{a}(\epsilon)$ and using Eq. 54 yields

$$\frac{\partial \sigma}{\partial a}\{\tilde{De}[\tilde{a}(\epsilon), \epsilon], \tilde{a}(\epsilon), \epsilon\} = 0. \tag{56}$$

Differentiating Eq. 53 with respect to ϵ (a fixed) gives

$$\frac{\partial \sigma}{\partial De}\frac{\partial \tilde{De}}{\partial \epsilon} + \frac{\partial \sigma}{\partial \epsilon} = 0. \tag{57}$$

Thus we have

$$\frac{\partial \tilde{De}}{\partial \epsilon}[a, \epsilon] = -\frac{(\partial \sigma/\partial \epsilon)}{(\partial \sigma/\partial De)}. \tag{58}$$

Differentiating Eq. 56 with respect to ϵ gives

$$\frac{\partial^2 \sigma}{\partial a \partial De}\left\{\left(\frac{\partial \tilde{De}}{\partial a}\frac{\partial \tilde{a}}{\partial \epsilon}\right) + \frac{\partial \tilde{De}}{\partial \epsilon}\right\} + \frac{\partial^2 \sigma}{\partial a^2}\frac{\partial \tilde{a}}{\partial \epsilon} + \frac{\partial^2 \sigma}{\partial a \partial \epsilon} = 0. \tag{59}$$

But from Eq. 54, we get

$$\frac{\partial^2 \sigma}{\partial a \partial De}\frac{\partial \tilde{De}}{\partial \epsilon} + \frac{\partial^2 \sigma}{\partial a^2}\frac{\partial \tilde{a}}{\partial \epsilon} + \frac{\partial^2 \sigma}{\partial a \partial \epsilon} = 0. \tag{60}$$

Solving for $(\partial \tilde{a}/\partial \epsilon)$, we find

$$\frac{\partial \tilde{a}}{\partial \epsilon} = \frac{-\left\{\frac{\partial^2 \sigma}{\partial a \partial \epsilon} + \frac{\partial^2 \sigma}{\partial a \partial De}\frac{\partial \tilde{De}}{\partial \epsilon}\right\}}{\frac{\partial^2 \sigma}{\partial a^2}}. \tag{61}$$

Also we may substitute from Eq. 58 to obtain

$$\frac{\partial \tilde{a}}{\partial \epsilon} = \frac{\frac{\partial^2 \sigma}{\partial a \partial De}\left\{\frac{\partial \sigma/\partial \epsilon}{\partial \sigma/\partial De}\right\} - \frac{\partial^2 \sigma}{\partial a \partial \epsilon}}{\frac{\partial^2 \sigma}{\partial a^2}}. \tag{62}$$

for constant δ.

Results and Discussion

A weakly nonlinear stability analysis for the case of a narrow-gap porous spiral channel is used to study the influence on Dean instabilities from the wall flux. Commercial spiral membrane modules belong to this narrow-gap case. Finlay et al. (1988) solved a weakly nonlinear problem for flow in a nonporous curved channel. This method is used here to obtain the vortex amplitude. In order to estimate the errors of the narrow-gap approximation and the weakly nonlinear stability analysis, the vortex amplitude A and the pressure gradient parameter Δp_g are compared with wide-gap and fully nonlinear stability analysis, respectively.

The difference between the present narrow-gap, weakly nonlinear analysis and the wide-gap fully nonlinear analysis

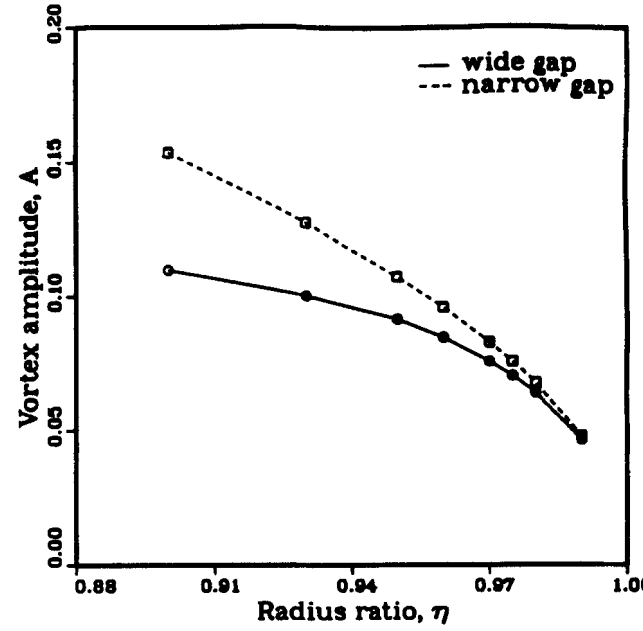

Figure 4. Vortex amplitude A from the wide-gap fully nonlinear (Finlay et al., 1988) vs. narrow-gap weakly nonlinear analysis for no wall flux at $a = 1.98$ and $De = 1.1De_c$.

(Finlay et al., 1988) in the case of no wall flux for the calculation of the vortex amplitude A is shown in Figure 4. The narrow-gap approximation always overestimates the vortex amplitude. The vortex amplitude for the narrow-gap approximation can be used within 20% error when the radius ratio η is greater than 0.95.

A measure of the strength of the vortices is the pressure gradient parameter Δp_g, defined as

$$\Delta p_g \equiv \frac{(\overline{\partial p}/\partial\theta) - (\partial P/\partial\theta)}{(\partial P/\partial\theta)} \tag{63}$$

where $-(1/r)(\partial p/\partial\theta)$ is the streamwise pressure gradient, $(\overline{\partial p}/\partial\theta)$ is the value of $(\partial p/\partial\theta)$ averaged over a computational box ($r_i \le r \le r_o$ and $0 \le z \le \lambda$), and $-(1/r)(\partial P/\partial\theta)$ is the streamwise pressure gradient for curved channel Poiseuille flow. By solving the θ-momentum equation for curved channel Poiseuille flow we obtain,

$$H \equiv \frac{\partial P}{\partial\theta} = -4\Big/\left[Re\left(r_c - \frac{(r_c^2-1)^2}{4r_c}(\ln\eta)^2\right)\right] \tag{64}$$

and

$$\frac{\partial p'}{\partial\theta} = h_0(t), \tag{65}$$

where

$$p'\left(\frac{\partial p'}{\partial\theta} = \frac{\overline{\partial p}}{\partial\theta} - \frac{\partial P}{\partial\theta}\right)$$

is the perturbed pressure. Also, h_0 is expanded with the vortex amplitude A,

$$h_0 = A^2(t)\left[h_{00} + \sum_{m=1}^{\infty} A^{2m}(t)h_{0m}\right]. \tag{66}$$

From Eqs. 63, 64, 65, and 66 we obtain to $O(A^2)$

$$\Delta p_g = \frac{h_{00}A^2}{H}, \tag{67}$$

where h_{00} is calculated according to Finlay et al. (1987).

The pressure gradient Δp_g is compared in Figure 5 as a function of the relative Dean number for the narrow-gap, wide-gap, and fully nonlinear wide-gap theories with no wall flux for $a = 1.98$ and $\eta = 0.975$. Below $De/De_c = 1.1$, the errors for the weakly nonlinear narrow- and wide-gap theories are within 30% and 20% of the fully nonlinear solution, respectively.

The change in the critical Dean number as a function of wall flux and wall-flux partition factor was calculated in Eq. 36. For equal suction through both walls, the critical Dean number is reduced. Thus for a given Dean number greater than critical, the vortex amplitude is increased according to Eq. 33. This effect is even larger when suction is only through the inner wall ($\beta = 1$). In contrast, when suction is only through the outer wall ($\beta = -1$) the critical Dean number increases and the vortex amplitude is reduced. For typical membrane wall fluxes and radius ratios on the order of $\eta = 0.99$ or less, the effect of wall flux on the critical Dean number is within 2% of the no-wall flux case. However, for radius ratios closer to 1 (larger radius of curvature) the effect can be much more significant.

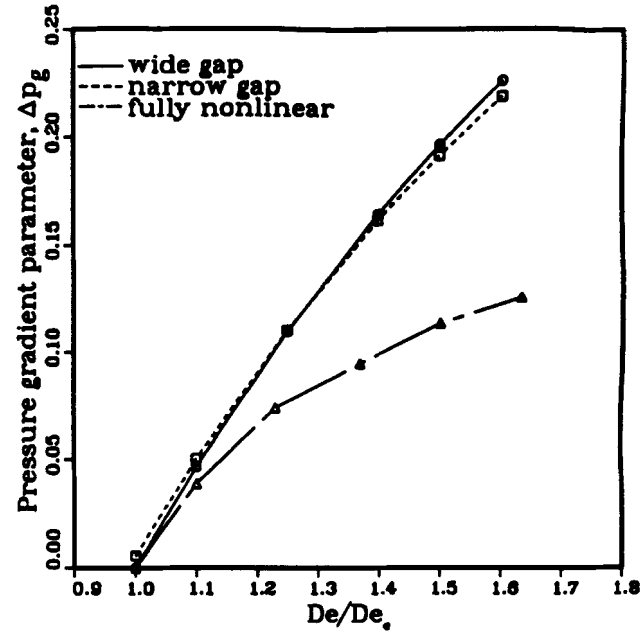

Figure 5. Pressure gradient parameter Δp_g from the wide-gap fully nonlinear (Finlay et al., 1988) vs. narrow-gap and wide-gap weakly nonlinear analysis for no wall flux at $a = 1.98$ and $\eta = 0.975$.

At Dean numbers greater than the critical Dean number, centrifugal instabilities cause a secondary flow containing streamwise-oriented Dean vortices. Dean vortices occur in regularly spaced counterrotating pairs. The contour plots for radial, total streamwise, and spanwise velocities at $\beta = 0$ (both walls equally permeable) are shown in Figures 6, 7, and 8, respectively. The maximum of streamwise velocity is displaced toward the outer wall; thus, the shear rate along the porous wall is greater at the outer than at the inner wall. Both the shear rate and presence of vortices promote solute mixing into bulk solution and reduce solute buildup on the membrane surface (Chung et al., 1994).

Further, we note that the value of the critical Dean number at the critical wavenumber, $\tilde{De}(\tilde{a}(\epsilon), \epsilon)$ may be approximated to leading order by neglecting the dependence on a. That is

$$\tilde{De}[\tilde{a}(\epsilon), \epsilon] = De_c(a_c) + \frac{\partial \tilde{De}}{\partial\epsilon}\epsilon = 0 \tag{68}$$

since by Eq. 54 $(\partial\tilde{De}/\partial a)|_{\epsilon}[\tilde{a}(\epsilon), \epsilon] = 0$. The evaluation of $(\partial\tilde{De}/\partial\epsilon)$ was discussed earlier (Eq. 36). Note that in the preceding discussion, the parameter δ is kept fixed.

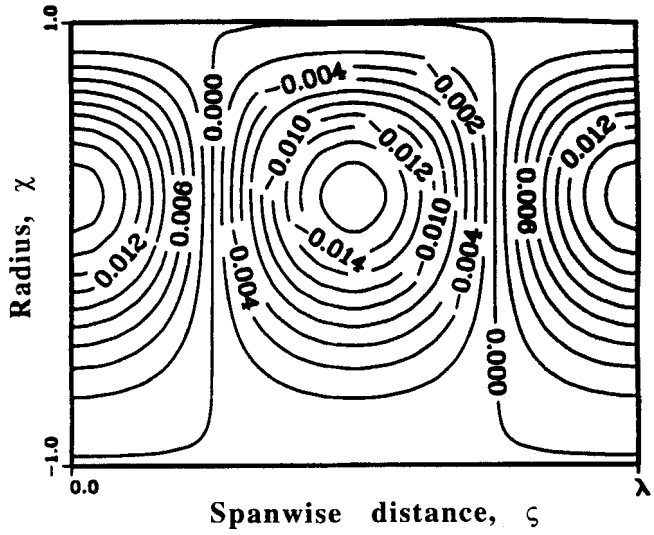

Figure 6. Contour plot of total radial velocity ($\bar{u}_1^0 + A * \bar{u}_0^1$) in an ($r, z$) plane at $De = 1.1De_c$, $a = 1.98$, $\beta = 0$, $\eta_I = 0.99$, and $\epsilon = 5 \times 10^{-5}$.

The perturbation $\tilde{a}_c(\epsilon) - a_c$ depends linearly on the wall-flux ratio ϵ for small ϵ and can be expressed as

$$\frac{\tilde{a}_c(\epsilon) - a_c}{\epsilon} = \frac{\partial \tilde{a}}{\partial \epsilon} \tag{69}$$

where $\tilde{a}_c$ and a_c are the critical wave number at the critical Dean number and at other Dean numbers, respectively. Assuming that

$$\sigma = \sigma^0 + \gamma_I \delta_I \sigma^1 + \cdots \tag{70}$$

from Eq. 32. Now

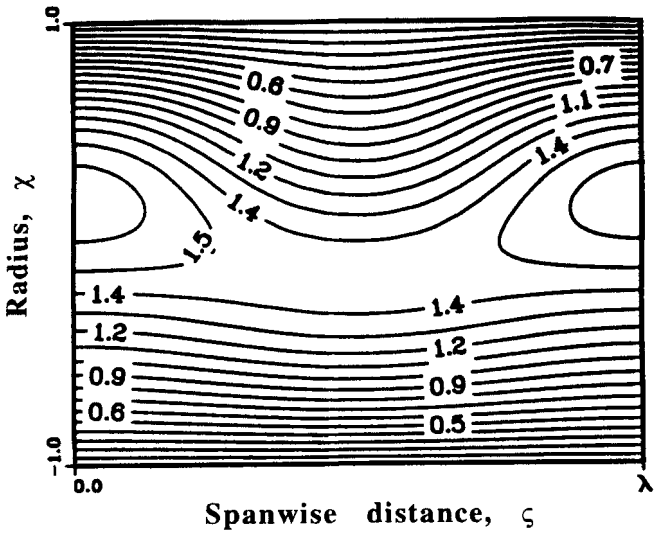

Figure 7. Contour plot of total streamwise velocity ($\bar{v}_0^0 + A * \bar{v}_0^1$) in an ($r, z$) plane at $De = 1.1De_c$, $a = 1.98$, $\beta = 0$, $\eta_I = 0.99$, and $\epsilon = 5 \times 10^{-5}$.

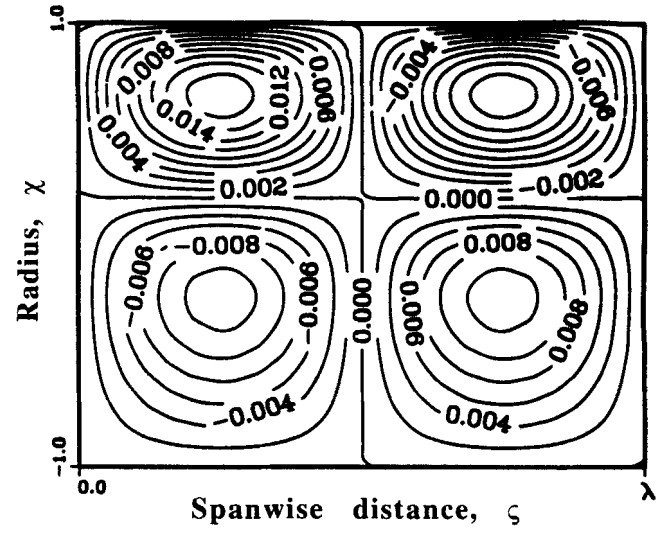

Figure 8. Contour plot of spanwise perturbation (or total spanwise) velocity ($A * \bar{w}_0^1$) in an (r, z) plane at $De = 1.1De_c$, $a = 1.98$, $\beta = 0$, $\eta_I = 0.99$, and $\epsilon = 5 \times 10^{-5}$.

$$\frac{\partial \sigma}{\partial \epsilon} \sim \frac{\sigma^1}{\delta_I} \sim \left(\frac{30}{\delta_I}\right)(1 + 2\beta) \tag{71}$$

from Eq. 36. Substituting for σ^1 from Eq. 71 into Eq. 70 and using the definition for ϵ, we obtain to order ϵ

$$\sigma = \sigma^0 + \left(\frac{30\epsilon}{\delta_I}\right)(1 + 2\beta). \tag{72}$$

We can now estimate the fractional perturbation, $\{[\tilde{a}_c(\epsilon) - a_c]/a_c\}$, at $a_c = 1.975$ and $De_c = 35.921$, where the step sizes are $\Delta a = 0.001$ and $\Delta De = 0.001$, $\epsilon = 5 \times 10^{-5}$, $\beta = 0$, $\eta_I = 0.99$, and $\delta_I = (1 - \eta_I)^{0.5} = 0.1$. Using difference approximations for the different terms in Eq. 62, the righthand side of Eq. 69 can be estimated (Anderson et al., 1984) as $(\partial \tilde{a}/\partial \epsilon) = 761.9415$, which gives $[\tilde{a}_c(\epsilon) - a_c] = 0.0381$ and the fractional perturbation, $[\tilde{a}_c(\epsilon) - a_c]/a_c = 0.01929$.

Conclusions

In summary, the velocity and pressure fields for flow in a (porous) spiral channel have been obtained using the narrow-gap approximation of the continuity and momentum equation. Spiral configurations based on the maintenance criterion for vortex formation were obtained. A U.S. patent based on this approach (Belfort et al., 1993) has been obtained. A weakly nonlinear stability analysis was used to study the influence of wall flux on the vortex amplitude and the pressure gradient parameter. Contour plots of the various component velocities for $De = 1.1De_c$ and predefined parameters were obtained. Wall shear rates are higher at the outer wall as compared to the inner wall. Some detailed conclusions are:

1. For equal suction through both walls ($\beta = 0$), the vortex amplitude A increases with the wall flux and the critical Dean number is reduced. This effect was even larger when suction was through the inner wall only ($\beta = 1$). In contrast, when

suction was only through the outer wall ($\beta = -1$), the vortex amplitude was reduced, and the critical Dean number was increased. Since in cases of practical interest for membrane filtration the amplitude of the wall flux is very small compared to the amplitude of the streamwise flow, this effect on critical Dean number is within 2% of the case without wall flux.

2. Simplification of the theory with the narrow-gap approximation always overestimates the vortex amplitude. The vortex amplitude with the narrow-gap approximation can be used with less than 20% error when the radius ratio η is greater than 0.95.

3. The behavior of the pressure gradient parameter Δp_g as a function of the relative Dean number is compared for the theory with the narrow-gap approximation, the wide-gap, and fully nonlinear wide-gap theories (Finlay et al., 1988) for $a = 1.98$ and $\eta = 0.975$. Below $De/De_c = 1.1$, the differences between the predictions for the weakly nonlinear narrow- and wide-gap theories are within 30% and 20% of the fully nonlinear solution, respectively.

In summary, a linear stability analysis and a formulation and solution of the weakly nonlinear problem with wall suction at one or both of the curved surfaces are presented. The fact that the result reverts to the nonporous wall case for low wall flux is also important. It means that prior solutions of vortex stability for the wide gap case are valid here, too.

Acknowledgments

The authors wish to express their appreciation for partial support of this research by Dow Chemical Company, Midland, Michigan, and their subsidiary, FilmTec Corporation, Minneapolis, Minnesota. Dr. Robert J. Petersen's (formerly of FilmTec Corp.) unflagging support is very much appreciated. The authors also thank Dr. Warren H. Finlay for providing the computer code for the weakly nonlinear analysis of the nonporous channel.

Notation

d = half channel width, cm
P = CCPF pressure (kg/m/s^2, Pa)
r = radial directional coordinate
r_i = inner spiral radius
r_c = centerline radius $[(r_i + r_o)/2]$
r_o = outer spiral radius
Re_c = critical Reynolds number
t = time, s
u = r-directional velocity
u_w = r-directional velocity at wall
v = θ-directional velocity
V = CCPF streamwise velocity
w = z-directional velocity
z = spanwise directional coordinate

Greek letters

ζ = dimensionless spanwise coordinate
γ = ratio of wall flux to gap width (ϵ/δ^2)
θ = streamwise coordinate
λ = spanwise wavelength of vortices nondimensionalized by d
μ = viscosity, g/cm/s
ν = kinematic viscosity, cm^2/s
ρ = density, g/cm^3
σ = growth rate for small amplitude disturbances
τ = dimensionless time $(t/d^2/\nu)$
φ = multivariable $(\gamma_I\theta)$
χ = dimensionless radial coordinate

Subscript

I = inlet

Literature Cited

Anderson, D. A., J. C. Tannehill, and R. H. Pletches, *Computational Fluid Mechanics and Heat Transfer*, McGraw-Hill, New York (1984).
Belfort, G., "Membrane Modules: Comparison of Different Configurations Using Fluid Mechanics," *J. Memb. Sci.*, **35**, 245 (1988).
Belfort, G., M. E. Brewster, and K. Y. Chung, "Curved Channel Membrane Filtration," U.S. Patent No. 5,204,002 (Apr. 20, 1993).
Belfort, G., and N. Nagata, "Fluid Mechanics and Cross-Flow Filtration: Some Thoughts," *Desalination*, **53**, 57 (1985).
Brewster, D. B., P. Grosberg, and A. H. Nissan, "The Stability of Viscous Flow Between Horizontal Concentric Cylinders," *Proc. R. Soc. A*, **251**, 76 (1959).
Brewster, M. E., K. Y. Chung, and G. Belfort, "Dean Vortices with Wall Flux in a Curved Channel Membrane System: 1. A New Approach to Membrane Module Design," *J. Memb. Sci.*, **81**, 127 (1993).
Brewster, M. E., K. Y. Chung, and G. Belfort, "Dean Vortices with Wall Flux in a Curved Channel Membrane System: 7. Optimizing Packing Density with a Variable Gap Spiral Wound Membrane Module," in preparation (1994).
Chandrasekhar, S., *Hydrodynamic and Hydromagnetic Stability*, Dover, New York (1961).
Chung, K. Y., "Instabilities of Viscous Flow in a Curved Channel: A New Approach to Membrane Module Design," PhD Dissertation, Rensselaer Polytechnic Institute, Troy, NY (1992).
Chung, K. Y., M. E. Brewster, and G. Belfort, "Dean Vortices with Wall Flux in a Curved Channel Membrane System: 3. Concentration Polarization in a Spiral Reverse Osmosis Slit," in preparation (1994).
Dean, W. R., "Fluid Motion in a Curved Channel," *Proc. R. Soc. London A*, **121**, 402 (1928).
DiPrima, R. C., *Nonlinear Partial Differential Equations*, Academic Press, New York, p. 19 (1967).
Drazin, P. G., and W. H. Reid, *Hydrodynamic Stability*, Cambridge Univ. Press, New York (1981).
Edelen, D. G. B., and A. D. Kydoniefs, *Linear Algebra*, American Elsevier, New York (1975).
Finlay, W. H., J. B. Keller, and J. H. Ferziger, "Instabilities and Transition in Curved Channel Flow," *J. Fluid Mech.*, **194**, 417 (1988).
Finlay, W. H., J. B. Keller, and J. H. Ferziger, Rep. TF-30, Dept. of Mech. Eng., Stanford Univ., Stanford, CA, p. 33 (1987).
Gibson, R. D., and A. E. Cook, "The Stability of Curved Channel Flow," *Quart. J. Mech. Appl. Math.*, **27**, 149 (1974).
Guo, Y., and W. H. Finlay, "Splitting, Merging and Wavelength Selection of Vortices in Curved and/or Rotating Channel Flow Due to Eckhaus Instability," *J. Fluid. Mech.*, **228**, 661 (1991).

Appendix

A summary of the equations of continuity and motion for flow in a spiral channel with porous walls and/or Dean vortices following the regular perturbation method described in the third section follows:

$O(A^0\gamma_I^0\delta_I^0)$

$$M_\theta: \quad \frac{De}{4\tilde{B}K}\frac{\partial \tilde{p}_0^{00}}{\partial \varphi} = D^2\bar{v}_0^0 \tag{A1}$$

$$M_r: \quad \frac{1}{2}(\bar{v}_0^0)^2 = \frac{\partial \tilde{p}_0^1}{\partial \zeta}. \tag{A2}$$

$O(A^0\gamma_I^1\delta_I^1)$

$$C: \quad \frac{\partial \tilde{u}_0^1}{\partial \zeta} - \frac{\bar{v}_0^0}{De} = 0 \tag{A3}$$

$$M_\theta: \quad D^2\bar{v}_0^1 = \frac{1}{2}De^2\tilde{u}_0^1 D\bar{v}_0^0 - \frac{1}{2}De(\bar{v}_0^0)^2 + \frac{De}{4\tilde{B}K}\frac{\partial \tilde{p}_0^{01}}{\partial \varphi}. \tag{A4}$$

$O(A^1\gamma_I^0\delta_I^0)$

$$M_\theta: \quad (D^2 - a^2 - \sigma^0)\bar{v}_1^0 = \frac{1}{2}De^2\tilde{u}_1^0 D\bar{v}_0^0 \tag{A5}$$

$$M_r: \quad (D^2 - a^2 - \sigma^0)(D^2 - a^2)\tilde{u}_1^0 = \frac{1}{2}a^2\bar{v}_0^0\bar{v}_1^0. \tag{A6}$$

$O(A^1\gamma_I^1\delta_I^1)$

$$M_\theta: \quad (D^2 - a^2 - \sigma^0)\bar{v}_1^1 - \frac{1}{2}De^2\tilde{u}_1^1 D\bar{v}_0^0 = \sigma^1\bar{v}_1^0 + \frac{1}{2}De^2\left(\tilde{u}_1^0 D\bar{v}_0^1 + \tilde{u}_0^1 D\bar{v}_1^0\right) - De\bar{v}_0^0\bar{v}_1^1 \tag{A7}$$

$$M_r: \quad (D^2 - a^2 - \sigma^0)(D^2 - a^2)\tilde{u}_1^1 - \frac{1}{2}a^2\bar{v}_0^0\bar{v}_1^1 = \sigma^1(D^2 - a^2)\tilde{u}_1^0 + \frac{1}{2}a^2\bar{v}_1^0\bar{v}_0^1 - \frac{1}{2}a^2De^2\left(\tilde{u}_1^0 D\tilde{u}_0^1 + \tilde{u}_0^1 D\tilde{u}_1^0\right) - \frac{\sigma^0}{De}D\bar{v}_1^0 + \frac{De^2}{2}\left(D\tilde{u}_0^1 D^2\tilde{u}_1^0 + \tilde{u}_0^1 D^3\tilde{u}_1^0\right) + \frac{1}{De}(D^3 - a^2D)\bar{v}_1^0. \tag{A8}$$

Note that Eqs. A1 and A2 describe CCPF (no vortices and no wall flux); Eqs. A3 and A4 describe CCPF with wall flux (no vortices and wall flux); Eqs. A5 and A6 describe Dean vortex flow without wall flux (Finlay et al., 1988); Eqs. A7 and A8 describe the interaction of Dean vortex flow with wall flux. It is possible to analytically integrate Eqs. A1 to A4.

Manuscript received Sept. 12, 1994, and revision received Mar. 13, 1995.